Check for updates

Determination and Evaluation of Saltwater Intrusion on Bafra Plain: Joint Interpretation of Geophysical, Hydrogeological and Hydrochemical Data

İsmail Demirci,[1] N. Yıldırım Gündoğdu,[1] M. Emin Candansayar,[1] Pantelis Soupios,[2] Antonis Vafidis,[3] and Hakan Arslan[4]

Abstract—Saltwater intrusion and its spatial distribution using a multidisciplinary approach were investigated on the northeast coast of Bafra Plain, which is one of the most important delta plains in Turkey. Intensive agricultural activity in the study area, which supplies the local and international market with agricultural products, is increasing the importance of this ecosystem. Even the groundwater potential and supply are high; the main problem is the groundwater degradation due to salinization. Moreover, local lithological, tectonic and hydrological complexities increase the uncertainty in the interpretation of the collected (chemical, geophysical, etc.) data, providing an inaccurate geomodel. Specifically, in the study area, there are mixtures of freshwater/saltwater aquifers and geological units containing clay lenses/thin layers and fine-grained alluvium. At the same time, these geological formations have similar resistivity responses, and the ambiguity of the collected electric and electromagnetic geophysical data is high. Therefore, a third geophysical method (seismic refraction), which is sensitive to different physical parameters to constrain the uncertainty in the interpretation, was used. In this study, the salinization of Bafra Plain and complex aquifer system was revealed with the combined use of direct-current resistivity and transient electromagnetic data constrained by seismic refraction data and guided by hydrogeological and hydrochemical data. Using information obtained from multidisciplinary study, we inferred that the intrusion is monitored inland up to 3.5 km. The intrusion is traced after approximately the first 10 m depth in the central part of the plain. Additionally, in some areas, it was concluded that the intrusion is interrupted by clay lenses. Also, drainage channels constructed in the plain have brought soil salinization under control but have not completely succeeded in controlling the saltwater intrusion into the deeper aquifer. The saltwater intrusion can move more inland if groundwater pumping is not controlled, especially in areas close to the river.

1. Introduction

The expected changes in global groundwater resources due to climate change and human population growth within the twenty-first century are immense (Vörösmarty et al. 2000; Milly et al. 2005; Clifton et al. 2010; Green 2016; Olivares et al. 2019). Coastal areas are densely populated, since they provide the best conditions for both economic development and quality of life, providing fresh water to more than one billion people living there (Small and Nicholls 2003; Post 2005). One of the most important environmental problems in coastal areas is the salinization of groundwater. Saltwater intrusion caused by overexploitation of groundwater, which upsets the sensitive hydrogeological balance between freshwater and seawater, is already affecting many areas on the earth (Post 2005; FitzGerald et al. 2008; Murgulet and Tick 2008; Barlow and Reichard 2010). Therefore, in order to anticipate and prevent intrusion in coastal areas, it is necessary to characterize the aquifer geometry and salinization borders of coastline aquifers.

Most of the agricultural plains, which are close to the coastline, are affected by irrigation-related groundwater problems. As in many other coastal aquifers, saltwater intrusion is a major problem in our study area in Bafra Plain, Turkey (Arslan 2013). Due to excessive use of fresh groundwater, the current balance between freshwater and saltwater is

[1] Geophysical Modeling Group, Department of Geophysical Engineering, Faculty of Engineering, Ankara University, 06830 Gölbaşı, Ankara, Turkey. E-mail: idemirci@eng.ankara.edu.tr
[2] CPG-Department of Geosciences, King Fahd University of Petroleum and Minerals, Dhahran, Saudi Arabia.
[3] Department of Mineral Resources Exploration, Technical University of Crete, Chania, Crete, Greece.
[4] Department of Agricultural Structures and Irrigation, Faculty of Agriculture, Ondokuz Mayıs University, Samsun, Turkey.

disturbed, and the intrusion interface moves more inland until a new equilibrium is established. The extent of the intrusion is affected not only by the ratio of groundwater pumping and its recharge, but also by the geological formations and hydraulic gradients (Kumar et al. 2016).

To protect soil and groundwater from salinization in Bafra Plain, the General Directorate of State Hydraulic Works (DSI) constructed irrigation and drainage canals in the 1990s. However, 25% of irrigation water is still supplied from hydro wells (Arslan and Demir 2011). Thus, due to excessive pumping in the plain, saltwater intrusion continues to be a problem. Arslan (2012) concluded that 72% of the area was under threat from salinity and recommended continuous quality monitoring of groundwater. The results of hydrochemical analyses of water samples obtained from shallow groundwater wells in the study area (Arslan et al. 2012) showed that the water quality was very good (drinkable and suitable for agricultural purposes). In contrast, water samples obtained from the deeper wells were reported to be of poor (high salinity) quality (Karaalioglu and Islam-oglu 1988; Cemek et al. 2007).

Available lithology logs from Bafra Plain provide important information on the geological formations and their complexities. Specifically, the study area is composed mainly of silty-clay, sandy-clay and clay formations. These data can provide some preliminary information about the saline/freshwater interface, but mapping of the spatial variability of the salinization front may fail in areas where sampling points are sparse and/or the geological complexity is high. Therefore, to clearly understand the mechanism of saltwater intrusion and define the salinization front, the integration of geophysical, hydrogeological and hydrogeochemical data must be applied (Burnett et al. 2002; Samsudin et al. 2008; Capizzi et al. 2010; Akpan et al. 2013; Kura et al. 2014; Redhaounia et al. 2015; Himi et al. 2017; Goebel et al. 2017).

Geophysical methods are important tools for groundwater studies, and especially in the case of saltwater intrusion surveys, information about the geometry of the aquifer and the interface between fresh/saline water can be estimated with high accuracy (Patra and Bhattacharya 1966; Soupios et al. 2010; Kanta et al. 2013; Vafidis et al. 2014;

Kourgialas et al. 2016; Demirci et al. 2017; Kalisperi et al. 2018; Rani et al. 2019). Due to the large resistivity contrast between seawater and freshwater in sandy, silty and gravelly formations (Archie 1942; Sabet 1975), geophysical electric and electromagnetic methods have been used by many researchers to map salinity in the subsurface (Foged et al. 2013; Wiederhold et al. 2013; Massoud et al. 2014; Soupios et al. 2015; Kourgialas et al. 2016; Demirci et al. 2017; Goebel et al. 2017). Among the available electromagnetic methods, transient electromagnetic (TEM) data have the highest sensitivity to conductive targets compared with the other geophysical techniques (Auken et al. 2010; Ezersky et al. 2011; Al-Garni and El-Kaliouby 2011; Khalil et al. 2013; Trabelsi et al. 2013; Yan et al. 2016; Kourgialas et al. 2016; Larsen et al. 2017; Golshan et al. 2018; Kalisperi et al. 2018; Ardali et al. 2018). In the study area, to determine the aquifer geometry and the salinity boundaries, direct-current resistivity (DCR) measurements were conducted. Due to the geological complexity of the area (clays mixed with sand, gravel at different sizes, and compaction), it was difficult to interpret the data obtained from a single geophysical method independently, and TEM data were collected to increase interpretation accuracy, especially in conductive media. DCR and TEM methods can provide the spatial and in-depth distribution of resistivity. However, the presence of geological units containing clays and silts can give similar resistivity responses. Consequently, it is sometimes difficult to distinguish between fresh and saline water within clay-based formations with an independent interpretation of DCR and TEM data (Kura et al. 2014; Demirci et al. 2017). Therefore, a third method, which is sensitive to different physical parameters, can be used, to distinguish units exhibiting close resistivity relations with each other. Interpretation of DCR and TEM data by constraining with seismic refraction (SR) data is a powerful tool in the identification of fresh and saline water within clay-based formations (Choudhury et al. 2001; Choudhury and Saha 2004; Wiederhold et al. 2013; Hamdan and Vafidis 2013; Demirci et al. 2017). Thus, SR measurements were collected at some sites to separate the clayey units.

The aim of this study is to develop an integrated systematic saltwater intrusion characterization methodology for monitoring the saline/fresh waterfront and planning effective prevention measures in coastal areas. This methodology is based on the joint use of geophysical data with logs and water samples to provide high-resolution information on the resulting local aquifer hydraulic behavior and groundwater pollution. For this purpose, the data obtained from the studies carried out beforehand (geological, hydrogeological, hydrochemical data) in the study area were re-evaluated together with the resistivity and velocity models acquired from multiple geophysical methods to obtain a detailed knowledge of salinity boundaries and aquifer geometry.

2. Study Area

Bafra is one of two major delta plains in the middle part of the Black Sea coast in Turkey. The plain is within the Samsun province boundaries. Kızılırmak River extends along the north–south direction and divides the plain into two pieces named as right and left coast. Especially in the right (Northeast) coast of the plain, previous studies have shown that saline water is present at boreholes near the waterfront (Arslan et al. 2007, 2012; Arslan 2013). In light of this information, the pilot survey area was selected between longitudes 35.91° to 36.09°E and latitudes 41.63° to 41.73°N with an area of approximately 40 km^2 (Fig. 1). Although irrigation and drainage canals have been constructed and operated by DSI since 1990, there is still a salinization problem in the study area, as mentioned above.

2.1. Geological and Hydrogeological Settings of Bafra Plain

From a geological point of view, Kızılırmak Delta (Bafra Plain) is a young area of about 2000 years. The elevation of the plain gradually increases to the south starting from the wide and flat alluvium area (Fig. 2).

The oldest geological unit that appears around the plain consists of the Upper Cretaceous-aged flysch series (Karaalioglu and Islamoglu 1988; MTA 2006)

(conglomerate, claystone, sandstone, marl interbedded with volcanic material) with an approximate thickness of about 3–4 km. Just above the flysch series, there is Eocene-aged flysch (sandstone, claystone, marl, conglomerate interbedded with volcanic material) and volcanic (andesite, basalt, tuff, agglomerate) series. These series host part of the groundwater within their fractures and fissures. The thickness of the series varies between 150 to 500 m in the field. The Neogene series, formed by the rivers entering the plain from the south, consists of clay, claystone, marl, sandstone, siltstone and conglomerate layers. From a hydrogeological point of view, it describes not only impermeable units but also permeable units on the plain, and its thickness is about 100–250 m (Karaalioglu and Islamoglu 1988).

Thirteen logs (drilled by DSI and Turkish Petroleum Corporation-TPAO) were used to characterize the lithology (Fig. 3) of the study area (Karaalioglu and Islamoglu 1988). From the hydraulic point of view, lateral and in-depth changes of clays (impermeable formations) make Bafra Plain a very complex hydrogeological environment. Leedshill et al. (1965) depicted the depth to the impermeable barrier (varied between 4 and 20 m) based on borehole information, but unfortunately, no digital data are available for any further use. In their reports, with the limited information obtained from boreholes, they claimed that the plain is covered with an impermeable barrier. However, the clay thickness and depths show significant changes and discontinuities (Fig. 3). Subsequent to their studies, Karaalioglu and Islamoglu (1988) introduced an up-to-date model that presents a complex hydrogeological scenario with different impermeable barriers.

From a hydrogeological point of view, the local aquifer is unconfined. Locally, artesian water was observed in only two deeper wells (L1318 and L4213). In the study area, there are many private wells belonging to local farmers, with depths varying from 5 to 20 m. The average depth of the water table is 4 m below the ground surface (Karaalioglu and Islamoglu 1988; Arslan and Demir 2011, 2013). These private wells pump water from the sandy and gravelly units of the alluvium. In addition, Arslan and Demir (2013) monitored the minimum and maximum depths of the groundwater table from the soil surface
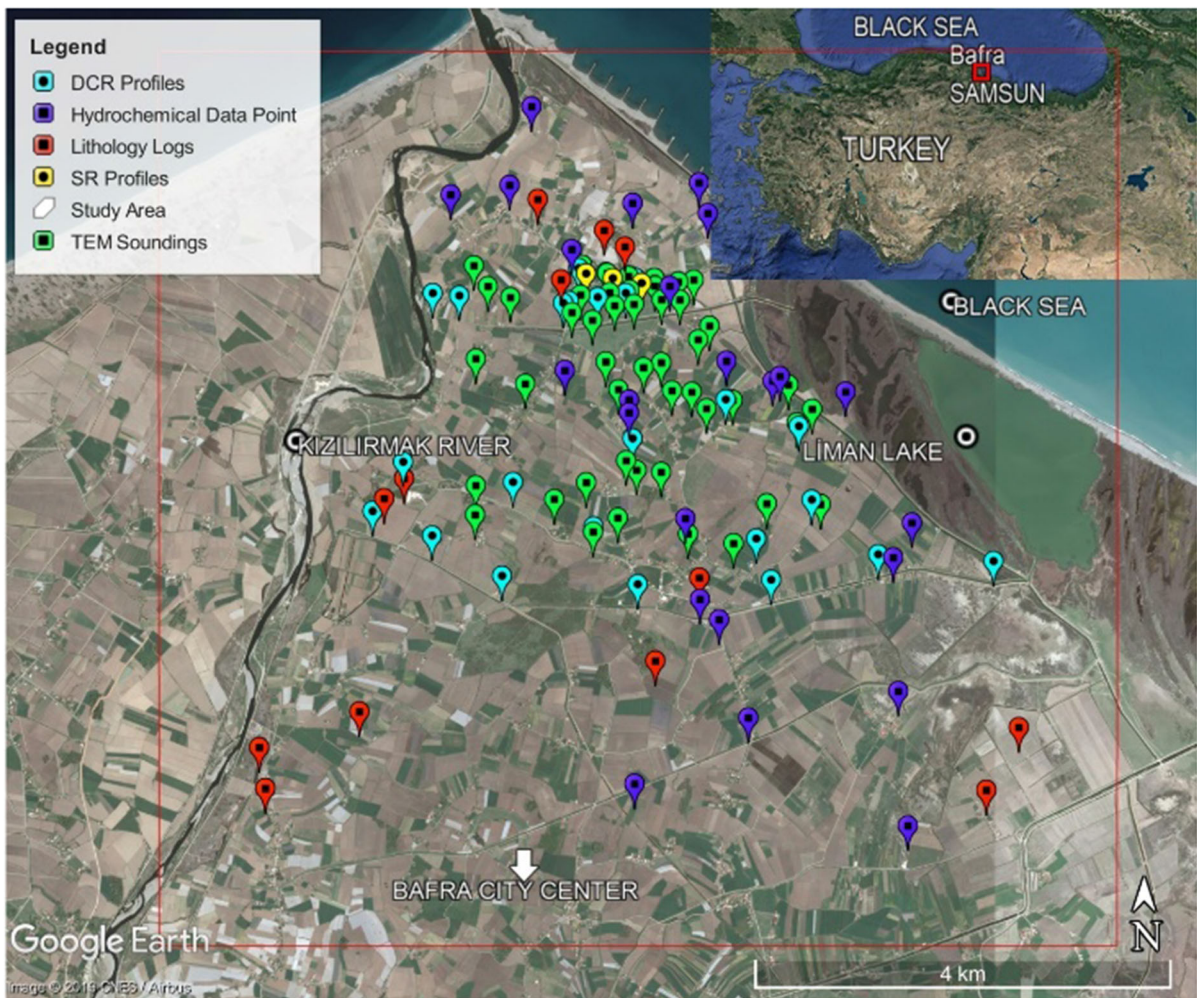
Figure 1
Location map of the study area with DCR, seismic refraction (SR), TEM measurement points, hydrochemical analysis and lithology logs

in every well. They conducted 32 groundwater table well observations and prepared groundwater level maps, concluding that the groundwater flow speed was low and that the groundwater level was below 4 m in 95% of the study area.

2.2. Hydrochemical Settings of Bafra Plain

Cemek et al. (2007) reported that irrigation deteriorated the salinity and alkalinity at Bafra Plain, the main reasons being extreme water use and insufficient drainage. In terms of evaluating the groundwater salinization, water samples from 24 different locations (Fig. 4) in the study area (Arslan

et al. 2007; Arslan 2013) were re-evaluated using the US Salinity Laboratory system. All samples were filtered with a 0.45 μm filter, sealed in polyethylene bottles and stored at 4 °C prior to analysis. The isotopic composition of water samples was analyzed at the Department of Technical Research and Quality Control of the General Directorate of State Hydraulic Works (DSI).

This water qualification system was first used to classify groundwater sources and their salinity levels in the plain (USDA 1954). The total concentration of soluble salts in water is referred to as the salinity hazard and is classified into low [electrical conductivity (EC) less than 250 μS/cm], medium
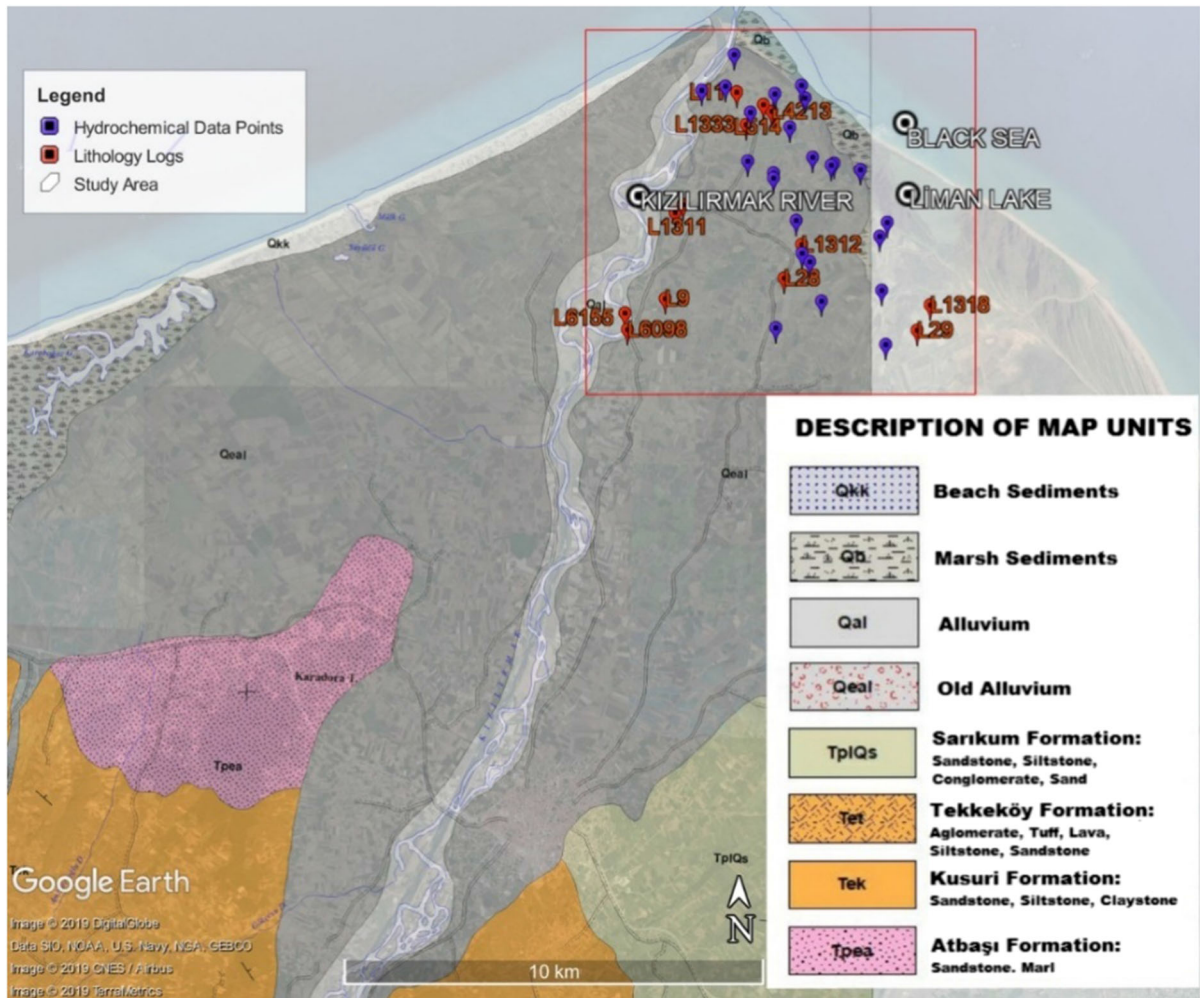
Figure 2
Geological map of the study area (the map is simplified from the Sinop-E35 quadrangle of the General Directorate of Mineral Research and Exploration: MTA 2006) The red rectangle shows the study area

(250–750 μS/cm), high (750–2250 μS/cm) and very high (greater than 2250 μS/cm). Total dissolved solids (TDS) analysis and EC measurements can be used in measuring salinity (Ayers and Westcott 1985). Sodium hazard is another classification mentioned in the same diagram and is classified as low, medium, high and very high for water having sodium absorption ratio (SAR) values of less than 10, 10–18, 18–26 or greater than 26, respectively. According to this classification scheme, groundwater with high EC values, with specific proportions of cations and anions and high SAR), is considered saltwater (Himi et al. 2017).

Fifty percent of the collected data show high to very high sodium hazard classes. According to the classification scheme mentioned above, if both of the hazards (salinity and sodium) are in the high or very high class, it is considered saltwater intrusion. It should be mentioned that the scenario of paleo-salinization has been abandoned, since the local geology and evolutionary history of Bafra Plain cannot support such a case. Moreover, sodium (Na^+), calcium (Ca^{2+}), magnesium (Mg^{2+}), chloride (Cl^-) and their molar ratios have also been used as an indicator of salinization (Somay and Gemici 2009). Specifically, the spatial changes of major ions,
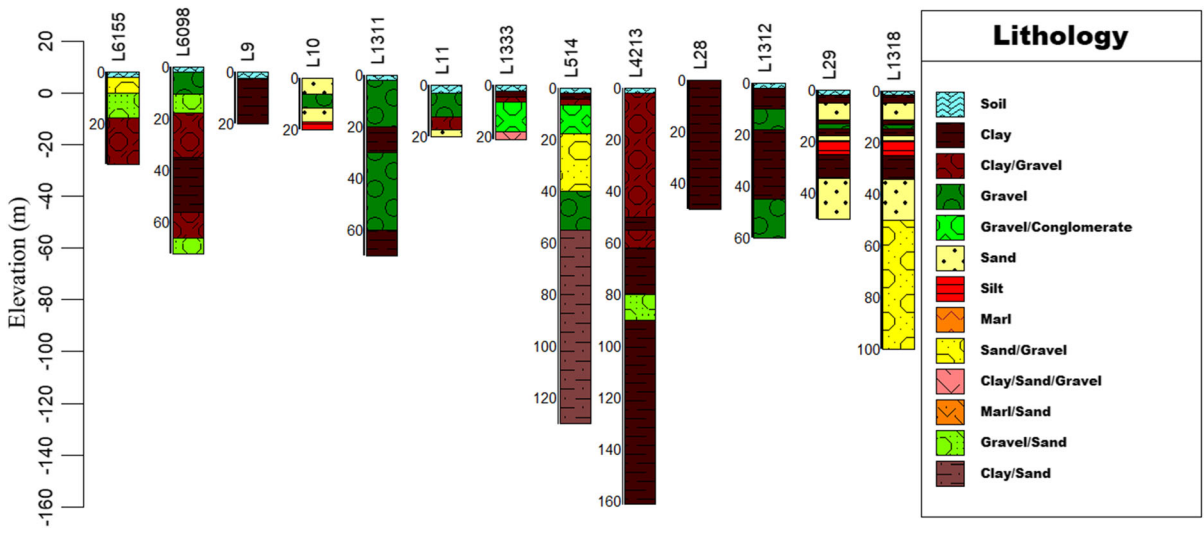
Figure 3
Lithological sections obtained from borehole logs in the study area [from west (left) to east (right)]
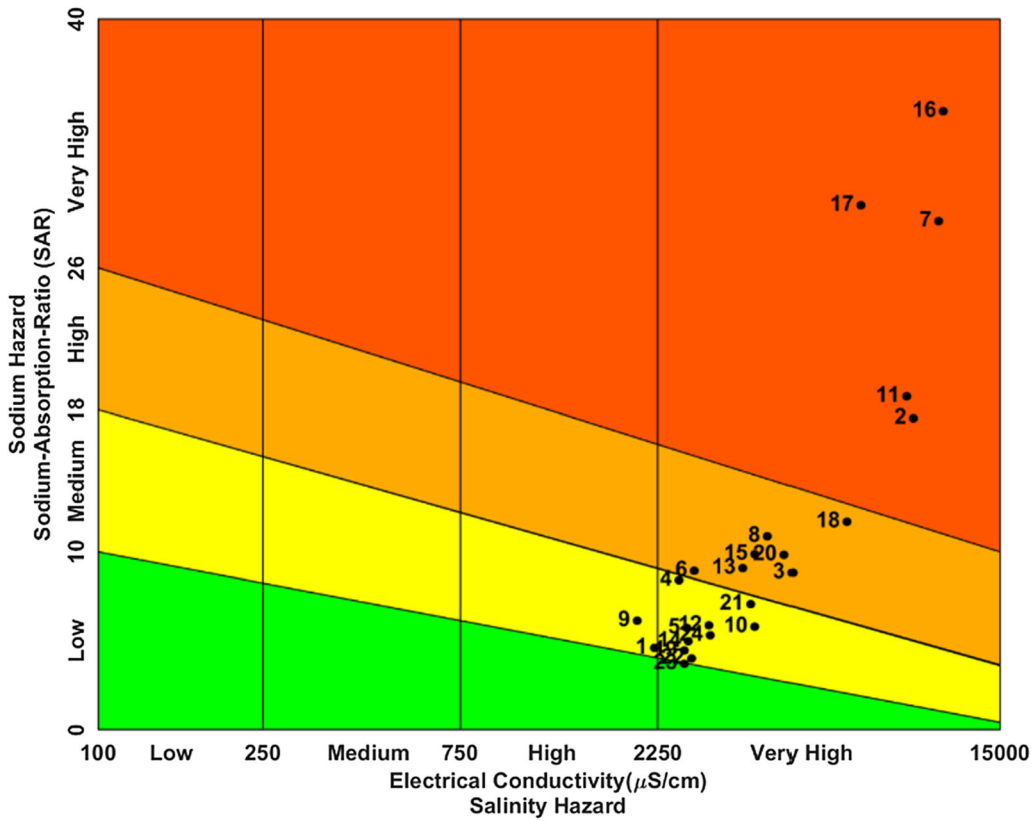

Figure 4
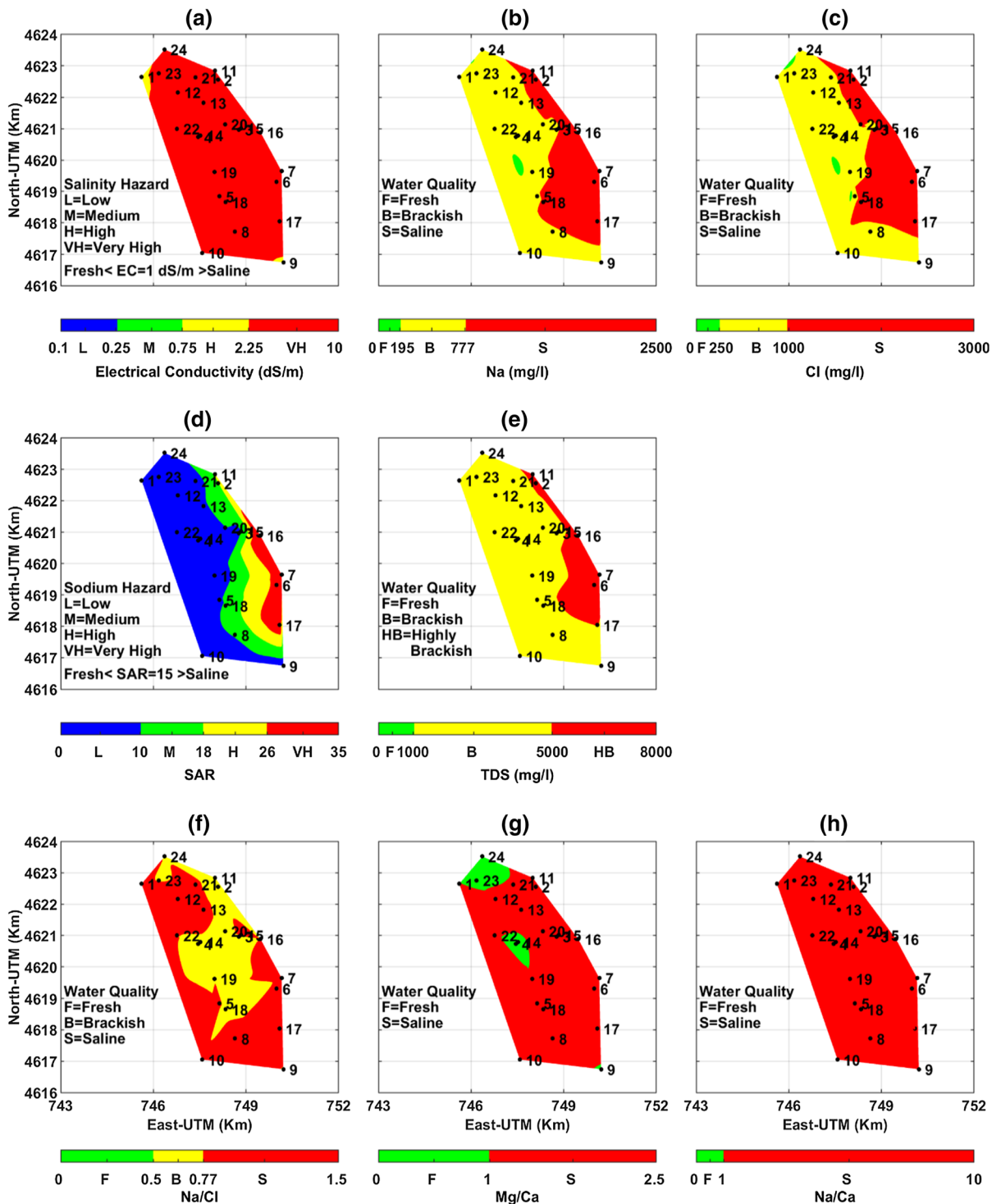Water classification of 24 groundwater samples collected in the study area

Figure 5
Maps of the major ions, proportions of ions, SAR, TDS and EC values in the study area: **a** electrical conductivity (EC) values, **b** sodium, **c** chloride, **d** sodium absorption ratio (SAR) values, **e** total dissolved solids (TDS) values and **f–h** the main ion ratios Na/Cl, Mg/Ca and Na/Ca which are used in the determination of saltwater intrusion, respectively

Table 1

The parameters used in the mapping of saltwater intrusion and the ranges in which they are defined

Parameter	Salinization criteria ranges	Type	References
EC	> 1 dS/m	Saline	Petalas (1997)
	< 1 dS/m	Fresh	
Na	> 195 mg/L	Saline	Somay and Gemici
	< 195 mg/L	Fresh	(2009)
Cl	> 250 mg/L	Saline	Andreasen and Fleck
	< 250 mg/L	Fresh	(1997)
SAR	> 15	Saline	EPA (1986)
	< 15	Fresh	
TDS	> 1000 mg/L	Saline	Martens and Wichmann
	< 1000 mg/L	Fresh	(2007)
Na/Cl	> 0.5	Saline	Nordstrom et al. (1989)
	< 0.5	Fresh	Somay and Gemici
	> 0.777	Saline	(2009)
	< 0.777	Fresh	
Mg/Ca	> 1	Saline	Somay and Gemici
	< 1	Fresh	(2009)
Na/Ca	> 1	Saline	Somay and Gemici
	< 1	Fresh	(2009)

proportions of major ions, SAR, TDS and EC values were mapped to evaluate the water salinization (Fig. 5). The salinization criteria used in the evaluation are given in the Table 1.

It should be mentioned that the presence of clays and marls (chemical composition of geological formations) in the study area is one of the factors that also increase the EC values of the waters. The average EC value of the Kızılırmak River feeding the plain is 1.35 dS/m (Arslan et al. 2012). However, the fact that the EC values obtained from the water samples are so high cannot be explained only by the effect of the geological (clayed) units and the Kızılırmak River (Fig. 5a).

The average salinity of seawater globally and in the Black Sea is about 3.5% (35 g/L) and 1.8% (18 g/L), respectively. Chloride and sodium are the main constituents of seawater, with average concentrations of 18.980 and 10.556 mg/L, respectively (Bashitialshaaer et al. 2009). Olutoge and Amusan (2014) reported that for the Black Sea, the average chloride and sodium concentrations were 9.500 and 4.900 mg/L, respectively. Because of the high concentration of sodium and chloride in seawater, their concentrations in groundwater samples are typically used as

indicators of saltwater intrusion into coastal aquifers (Martens and Wichmann 2007). On the other hand, sodium is often naturally found in groundwater, because most rocks and soils contain sodium compounds from which sodium is easily dissolved. However, no significant sodium-containing minerals were found in the study area (Karaalioglu and Islamoglu 1988; MTA 2006; Güler et al. 2014). For this reason, we considered that it was possible to correlate the sodium and chlorine content in the water samples directly with saltwater intrusion (Fig. 5b, c). If we look at SAR (SAR values make more sense when considered in conjunction with the EC values—shown in Fig. 4) and the TDS spatial distribution map (Fig. 5e), the present relationship can be similarly observed with sodium and chlorine. In addition, the Na/Cl, Mg/Ca and Na/Ca molar ratios for the whole study area show consistently high values (Fig. 5f–h, respectively). Only the Na/Cl molar ratios are slightly different from the other molar ratios. If seawater intrudes into a freshwater aquifer, the molar ratio of the Na/Cl in groundwater is increasingly changed along the mixing line because of the chemically conservative behavior of chloride. Somay and Gemici (2009) reported that most of the saline groundwater samples taken from the coastal area showed some depletion of Na through ion exchange reactions during the mixing process. In order to identify the salinization, Nordstrom et al. (1989) and Somay and Gemici (2009) used Na/Cl molar ratios of 0.5 and 0.777, respectively. In our study, the Na/Cl value in the water quality map related to saltwater was higher than 0.5 units; however, we considered a different classification of the zone (named brackish) in the map where the values varied between 0.5 and 0.777, which was compatible with both studies. For this interpretation, we correlated this data with other molar ratios and made a similar interpretation. Considering all the hydrochemical data, we determine that the regions of the study area close to the Kızılırmak River and the drainage channels could be thought of as a mixture zone. However, based on all hydrochemical analysis carried out, saltwater intrusion was observed to be present in the entire study area when all parameters were considered together (Fig. 6). As such, we classified and mapped the probability of salinization using salinization criteria
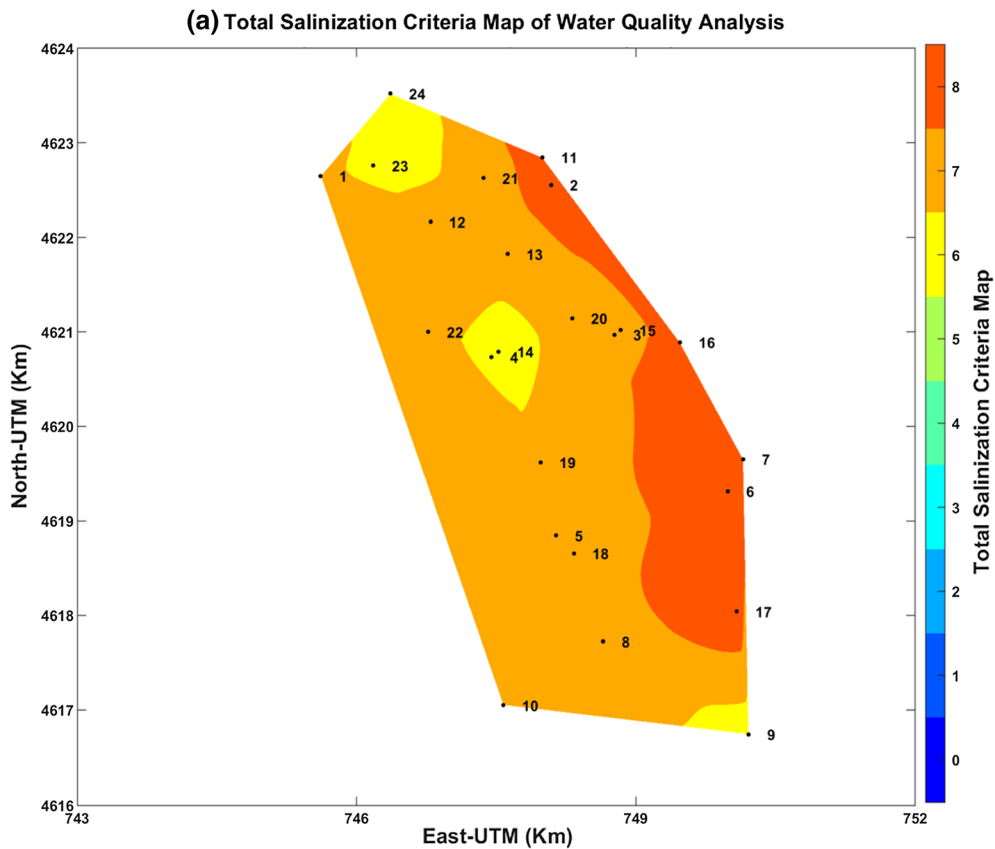
Figure 6
Probability map of total salinization criteria obtained from water quality analysis. Water sampling locations (dots) area also shown

ranges in Table 1. In this mapping, if the parameter value is below the associated salinity criteria, we used 0 (fresh) as the possibility value; otherwise, we used 1 (salty). With summation of the possibility of salinization values, we have mapped how many of the 80 salinity criteria corresponded to intrusion. In Fig. 6, zero (0%) indicates freshwater, and 100 (100%) indicates that all the salinization criteria in Table 1 are met. We saw that a minimum of six criteria pointed to saltwater intrusion for all hydrochemical analyses carried out in the field. Accordingly, based on all collected hydrochemical data, we can conclude that the probability of saltwater intrusion in the study area is greater than 75%. In addition, it was observed that the hydrochemical data, which did not meet the salinity criteria, were very close to the limit value, which is shown in Table 1 as salinization criteria ranges.

3. Geophysical Studies in Bafra Plain

In the study area, DCR, TEM and SR data were collected at the northern-eastern part of Bafra Plain, covering an area of about 40 km^2. The main purpose was to map the front of the saltwater intrusion by joint interpretation of geophysical, geological, hydrogeological and hydrochemical data. Data from 24 DCR sounding profiles, 47 TEM soundings and three SR profiles were acquired in the study area.

3.1. Direct-Current Resistivity (DCR) Method

To characterize the vertical and lateral extent of aquifer formations, resistivity models from the inversion of 24 DCR sounding-profiling data sets were obtained. The profile's length and the electrode spacing were 275 and 5 m (56 electrodes were used),
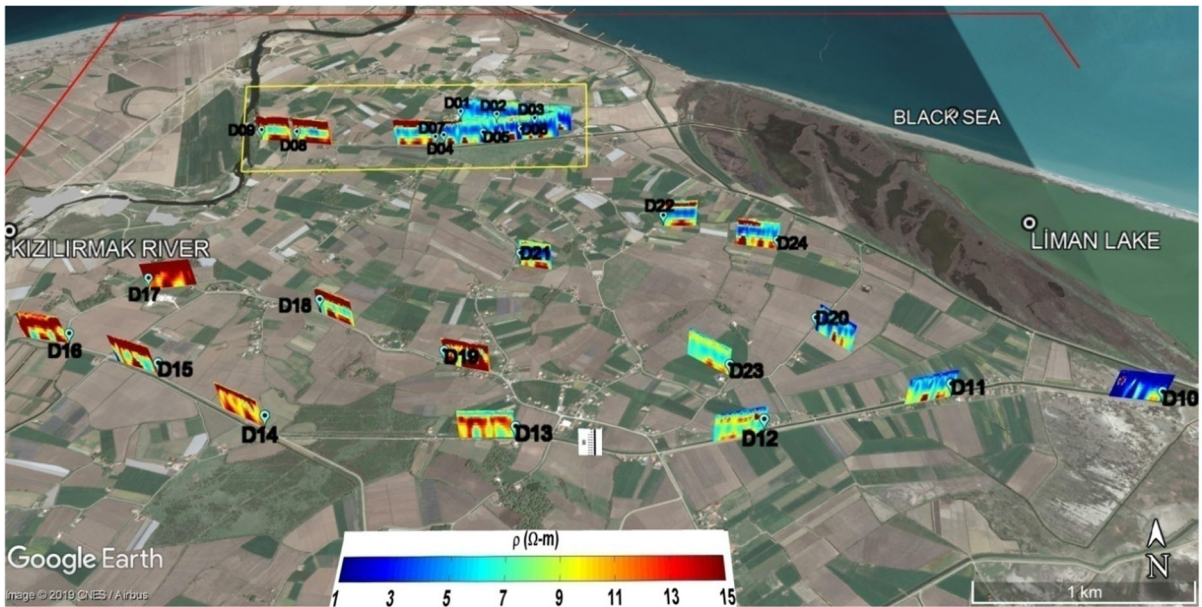
Figure 7
The resistivity models obtained from the inversion of 24 profiles of DCR data superimposed on a Google Earth map
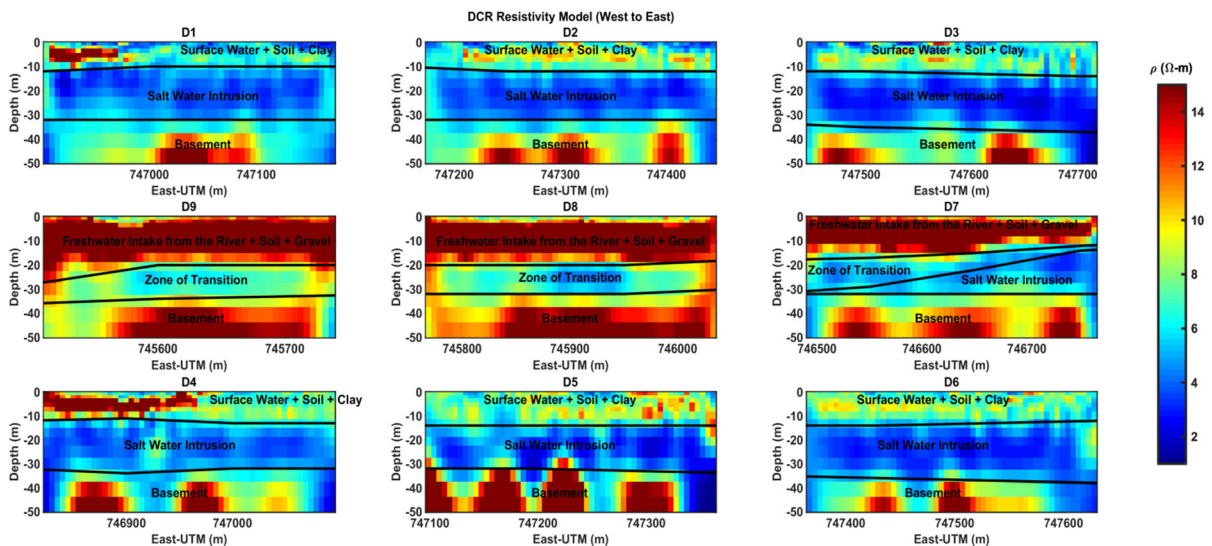

Figure 8
Interpreted resistivity models obtained from the inversion of 9 profiles of DCR data (yellow rectangle in Fig. 7)

respectively. All DCR profiles were collected using both Schlumberger (Sch) [depth of investigation (DOI): 65 m] and dipole–dipole (DD) (DOI: 55 m) configurations to increase both vertical and horizontal resolution, respectively. Apparent resistivity data

were collected with an AGI SuperSting R8/IP system. In this study, the inversion algorithm developed by Demirci et al. (2012) was used to obtain the final resistivity models obtained from joint inversion of both data sets (Sch-DD). The root-mean-square
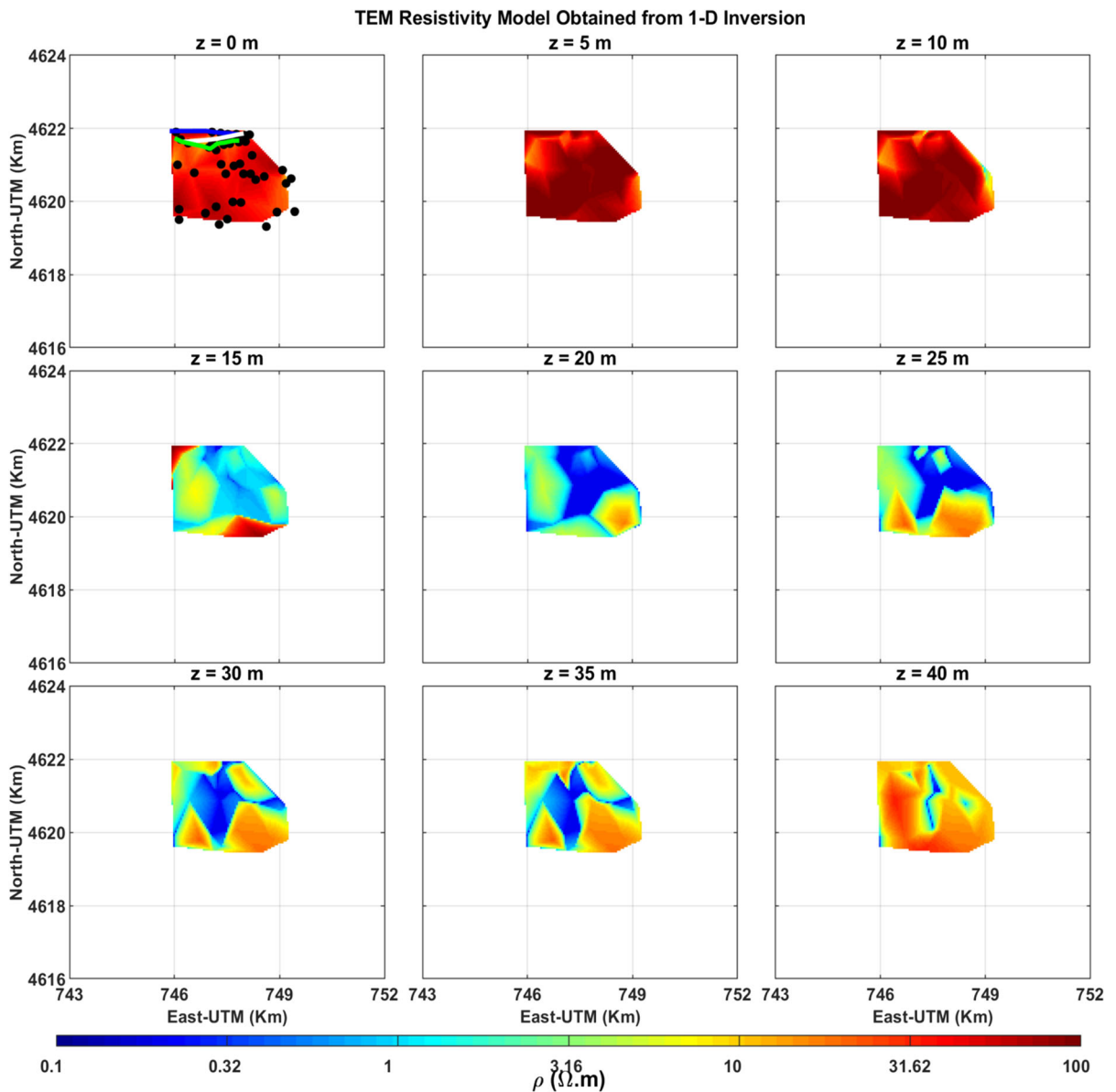
Figure 9
Pseudo-3D (spatial distribution of resistivity at different depths) resistivity maps obtained from the interpolation of 1D inversion of TEM data (blue, white and green lines in the $z = 0$ m plot depict pseudo-2D TEM resistivity profile 1, profile 2 and profile 3, respectively)

(RMS) error computed (after 6–10 iterations) for all 24 DCR profile data varied between 1.6 to 5.5%.

The spatial and depth distribution of resistivity resulting from the inversion of 24 profiles of DCR data was superimposed on a Google Earth map and is shown in Fig. 7 (in all sections, the maximum depth of investigation and the model parameter thicknesses

in the vertical direction are kept the same). A pattern of three geoelectrical layers is observed in all resulting DCR cross sections. The seawater intrusion is clearly mapped and interpreted at the northern and eastern part of the study area, as seen in the yellow rectangle in Fig. 7. This pattern can be clearly identified in the interpreted resistivity models in
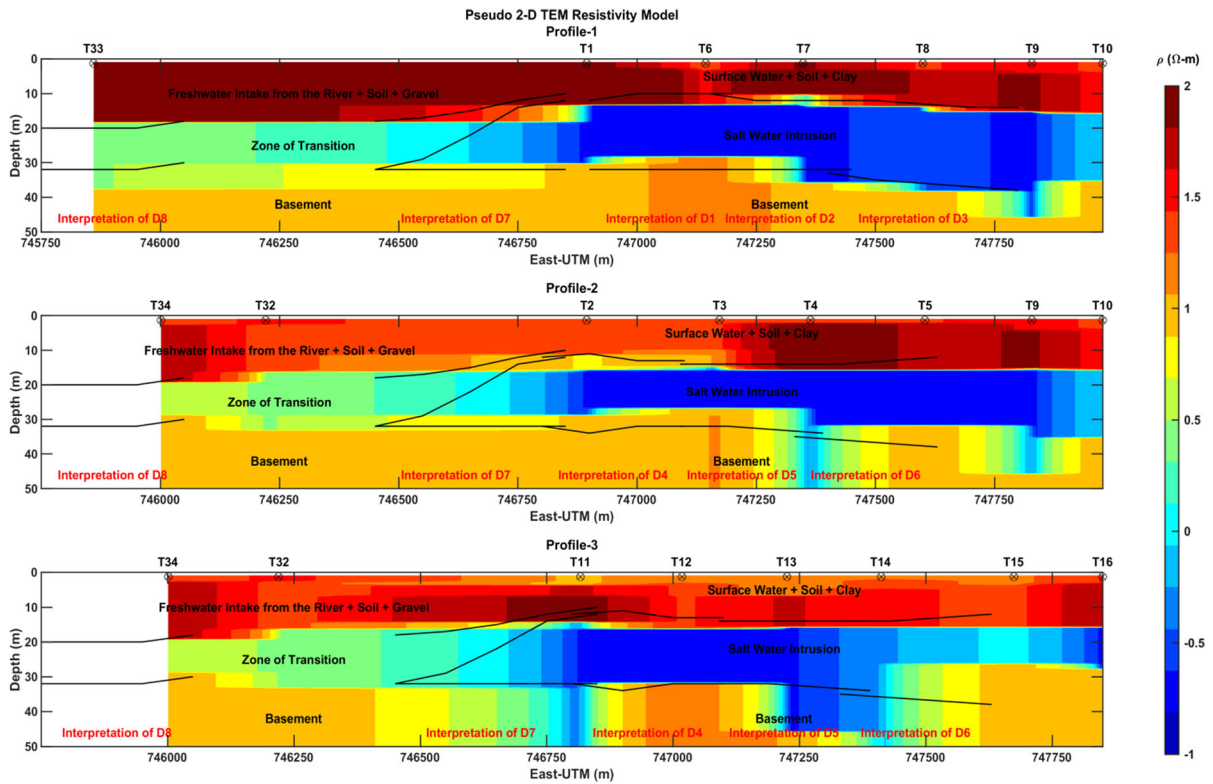
Figure 10
Pseudo-2D TEM resistivity models, which are close to profiles in Fig. 8 (black lines indicate interpretation obtained from DCR profiles)

Fig. 8. In the south and southwestern part of the study area (in Fig. 7, lower left corner), the saltwater interference is reduced along with the recharge from the Kızılırmak River. In addition, the aquifer structure, which is clearly seen with the bluish colors in Fig. 7, is deepened from the northeast to the southwest. Seawater can be thought to mainly intrude throughout the intermediate geoelectrical layer, which is related to this aquifer structure since it exhibits very low resistivity values ($< 4\ \Omega$ m). Its thickness is mainly less than 15 m, but exceeds 40 m in some places. The first layer lacks lateral homogeneity, and its thickness, in general, does not exceed 20 m. Both the first and third geoelectrical layers are characterized by relatively higher resistivity values ($> 7\ \Omega$ m). Based on the available logs, the first geoelectrical layer can be associated with dry and semi-saturated soil, clay, and sandy and gravelly units of the alluvium. The last geoelectrical layer represents sand-gravel units with high clay content bounded from the top by an impermeable clay band. Interpreting the DCR data together with geological and hydrogeological data, it is seen that the impermeable clay materials were observed to be dominant toward the southern part of the area, and the saltwater intrusion is minimal in these areas. To show the saltwater intrusion mechanism, nine DCR profiles, which are close to each other and close to the shore (yellow rectangle in Fig. 7), are mapped as presented in Fig. 8. Profiles 3 and 6 are about 1 km from the Black Sea, and profile 9 is 3.5 km from the Black Sea and ends close to the Kızılırmak River. In the eastern part of the study area, the depth of the groundwater table is approximately 15 m, and the bottom of the aquifer extends to a depth of 40 m. In the western part of the study area, which is close to the river, hydrostatic equilibrium can be observed between saltwater and freshwater, and it can be seen in the interpreted cross sections. In addition, in Fig. 8, resistivity values ranging from 4 to 6 Ω m in profile 8
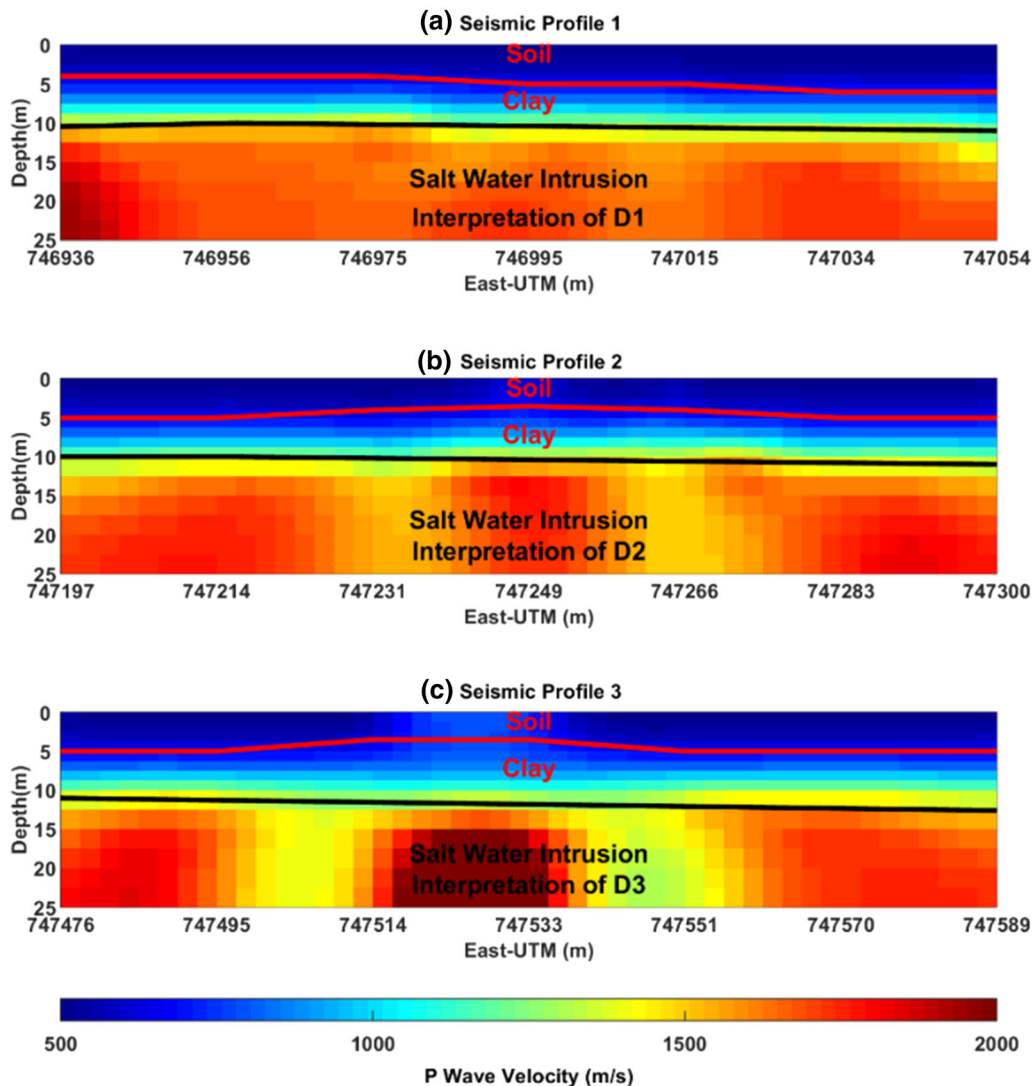
Figure 11
Inverted P-wave velocity model of SR data collected along the first three DCR profiles: **a** profile 1, **b** profile 2 and **c** profile 3

and profile 9 are interpreted as a mixing zone between the freshwater and saltwater.

3.2. *Transient Electromagnetic Method (TEM)*

In this study, TEM data were collected for 47 stations using the Zonge GDP-32 system with central loop configurations. We used a 50 m × 50 m rectangular wire as a transmitter loop and an induction coil as the receiver. The depth of investigation was approximately 100 m for each TEM sounding. To

calculate the 1D resistivity models, WinGLink software (Geosystem, Italy) was used. In all inversions, the number of layers in the obtained 1D resistivity models ranged from three to five. The final RMS error (after 6–20 iterations) for the TEM data of all 47 stations was between 1.2 and 4.8%.

The final inverted 1D resistivity models of TEM data from 47 stations are interpolated and mapped for different depth levels (depth slices) in Fig. 9. The pseudo-3D resistivity model deduced from 1D inversion of TEM data indicates increased salinity (low

resistivity values $< 1\ \Omega$ m) in the northern and eastern parts of the studied area. With this map, the spatial distribution of saltwater intrusion can be easily traced. In these depth slices, light green and blue colors depict saltwater zones. In the DCR resistivity models, the resistivity of this layer was found to be higher than in the TEM resistivity models. The fact that the resistivity values of the units in the working area are very close to each other, and that the conductivity of the units in the field is generally high, makes it difficult to interpret the results of the DCR method, which is more sensitive to the resistive structures. Therefore, the inverted resistivity models produced from the measured DCR data cannot fully obtain the resistivity values of the conductive structures. Thus, the layer that was interpreted as the saltwater intrusion in the DCR cross sections can only be verified using the TEM data.

To understand the relationship between DCR resistivity models in Fig. 8 and the TEM resistivity models, Fig. 10 was created, which is shown in blue, white and green lines in Fig. 9. Interpretations made for DCR cross sections were plotted on pseudo-two-dimensional (2D) TEM cross sections in Fig. 10 with black lines. When we look at the TEM resistivity cross sections, a pattern of three geoelectrical layers is mainly observed, similar to DCR resistivity models. When interpreted together with DCR data, it can be seen that the aquifer roof depth and the fresh/saltwater transition zone can be detected, and we can conclude that both models are in good agreement.

3.3. Seismic Refraction (SR) Method

SR data were collected along three of the DCR profiles to obtain additional geophysical data and to accurately evaluate the saltwater intrusion. SR data were collected along three of the DCR study lines in order to distinguish the clayey zones from the salinization. A multi-channel Geometrics StrataView system was used to acquire the seismic profiles. Forty-eight (14 Hz) geophones spaced every 2.5 m
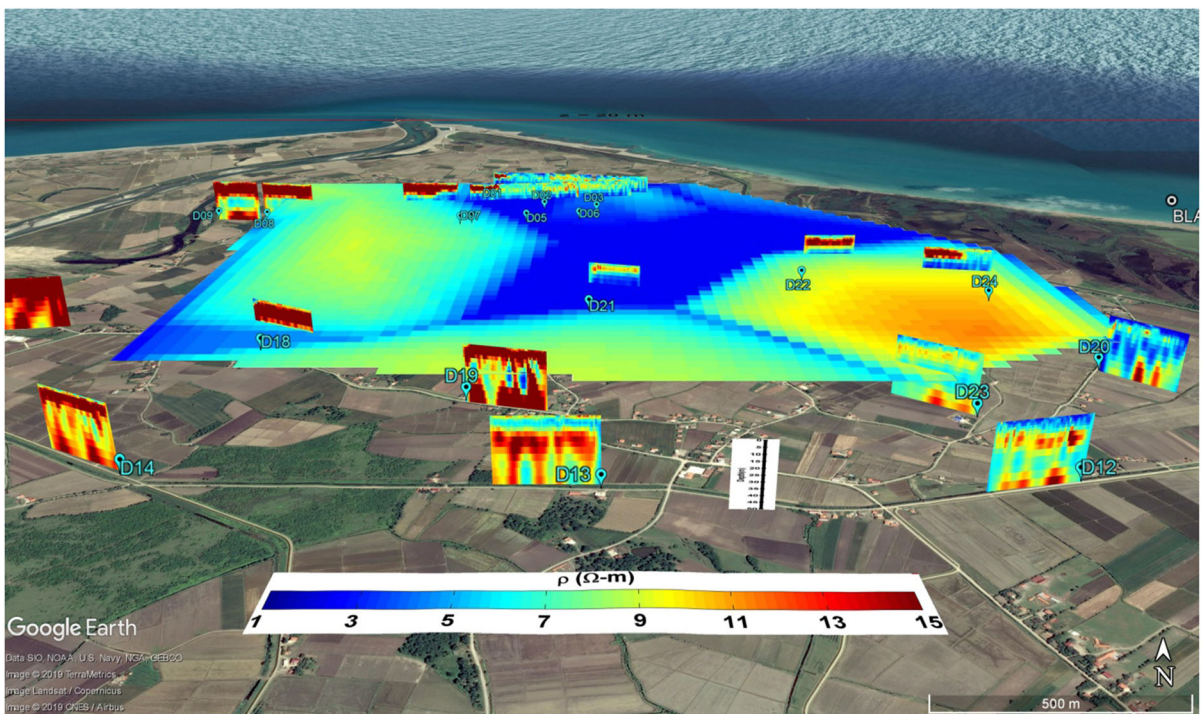

Figure 12
Joint presentation of DCR cross sections and TEM depth slice (for $z = 20$ m)

were used to collect data from 18 shot points per profile. The total length of each profile was 117.5 m.

Saturated sand and gravel P-wave velocity is generally changing between 1500 and 2000 m/s. Unsaturated clay units give low seismic velocities, and water-saturated clay units give high seismic velocities from this range (Choudhury et al. 2001; Choudhury and Saha 2004). Taking advantage of these differences to interpret low-resistivity structures in the plain, SR measurements were collected along three DCR profiles.

Seismic data were processed using the 2D SR tomography algorithm developed by Demirci et al. (2017). In all inversions, SR data were sensitive to first 20 m depth (based on ray path coverage on the last iteration). The RMS error computed for the last iterations (8–10 iterations of all three profiles) was found to vary between 1.2 and 3.2%. Figure 11 shows the interpreted 2D velocity models obtained from the SR data. In Fig. 11, black lines indicate interpreted structural boundaries of related DCR profiles, and red lines indicate interpretation obtained with SR data considering the DCR resistivity and lithology logs. Based on the resulting P-wave velocity models, three layers are mainly observed on SR cross sections. Considering the DCR resistivity models, if we relate the geological units to the velocity layers, the first layer may be associated with soil (ranging from 400 to 700 m/s), the second layer may be interpreted as clay and clayey sand and gravel units (ranging from 700 to 1500 m/s), and the last layer may be thought to represent the aquifer contaminated with saltwater (ranging from 1500 to 2000 m/s).

4. Discussion

In Bafra Plain, the clay units are located at shallow depths on the south part of study area with increasing thickness (look at L9, L28, L29, L1312 and L1318 in Fig. 3). The clayey geological structure in this section prevents the saltwater intrusion from moving further into the interior and acts as a barrier. It is similarly observed in DCR resistivity sections (D12, D13, D14 and D19) and TEM resistivity models corresponding to these locations that the resistivity values are above 7 Ω m, and it can be

inferred that there is no occurrence of saltwater intrusion (see Fig. 12).

The D12, D13 and D23 DCR resistivity sections are close to the L1312 lithology log (approximately 500 m from the profiles). In L1312, clayey units with gravel bands can be observed (its thickness is approximately 10 m), and it is possible to correlate geological units with the related resistivity sections (profiles D12 and D23 are interpreted as clay, gravel, clay and gravel from top to bottom, respectively). The D13 profile exhibits similar behavior as the D12 profile. The relative thickness of the clay decreases westward from these profiles (see D15, D16, D17 and D18 DCR profiles and L10 and L1311 lithology logs) and increases toward the south (look at L28 and L9 lithology logs).

In the southwest section of the study area, lithology logs (L10 and L1311) show sandy and gravelly units in the first 20 m and between 30 and 60 m, respectively. In addition, it can be seen that the silty and clayey levels limit the top and bottom of the second sandy and gravel units (thickness of about 10 m). The D16 and D17 DCR resistivity sections are very close to the L10 and L1311 lithology logs (approximately 100 m from the profiles), respectively. In these resistivity sections, the upper sandy and gravelly units exhibit greater resistivity values of 15 Ω m. Sandy and gravelly units contain highly variable amounts of both dispersed and interbedded clays, and the aquifer structure is thought to be composed of sandy and gravelly units, which contain a high percentage of clays, between clay bands. In light of this information, low-resistivity layers (resistivity values between 5 and 15 Ω m) in the related resistivity sections (D15, D16, D17 and D18 DCR profiles and T31, T35, T36 and T37 TEM stations) can be designated as clay, sand/gravel, clay intercalation about 25 m in thickness. Due to the relatively thick clay bands (L10 and L1311) and high clay content of the gravelly aquifer structure in comparison with the northern side of the area (L11, L514, L1333 and L4212) and recharge from the Kızılırmak river, saltwater intrusion is prevented in these parts of the study area. In addition, it can be inferred that these structures with the decreasing clay band thicknesses and clay content constitute the aquifer structure observed in the northern part (see Fig. 12).

In the north and east direction, there is a remarkable decrease in the resistivity values as the study field approaches the coast. These low-resistivity measurements are attributed to clay deposits and seawater intrusion. In D1, D2, D3, D4, D5, D6, D7, D10, D11, D20, D21, D22 and D24 DCR resistivity models, both clay and saline fluids reduce the bulk resistivity of the aquifer, and these resistivity values are below 4 Ω m in Fig. 7. It is expected that the resistivity values of sandy and gravelly units with higher clay content will decrease. However, it is not possible to link this drop only with clay content and clayey levels (Farid et al. 2014). In the measurements made in the southeastern part of the plain, it can be concluded that the relative low-resistivity values of the relevant units indicate the presence of saltwater intrusion. In order to strengthen the interpretation, TEM and SR measurements were taken, and the obtained resistivity and velocity models support the interpretation made for the study area. As a result of these measurements, it can be inferred that low resistivity values of 1 Ω m and high seismic velocity values of 1500 m/s observed in the inverted models indicate saturated units with saline water.

In all the TEM and DCR resistivity sections, into the uppermost resistivity layer (approximately the first 20 m from the surface with resistivity values greater than 15 Ω m), the resistivity values decrease from the Kızılırmak River toward the coastline (Fig. 12). The resistivity values, which are generally observed to be low in gravelly and sandy units in the region, are associated with both high clay content and fresh/saltwater inputs. In order to interpret this observation, preliminary work on the area was reviewed, and interviews with local farmers were conducted. In the study area, Arslan and Demir (2013) monitored 32 groundwater table observation wells and mapped the groundwater level. They observed that the groundwater level was below 3 m, and it flowed from the Kızılırmak River toward the Black Sea with low flow speed. Moreover, local farmers reported that the water obtained from the shallow groundwater wells (up to 10 m) was used as drinking water and for agricultural purposes (it is brackish or slightly fresh), but the water obtained from the deeper wells was of poor quality. Because of these hydrological data and observations, it is

interpreted that this resistive layer is the upper sandy and gravelly aquifer layer fed by the river. It is observed that this layer sometimes contains relatively thick clay bands and even sometimes with the hydrostatic equilibrium preserved throughout up to the inner zone. The decline in the resistivity of this layer as it approaches the coastline can similarly be explained by limited saltwater intake. However, it is thought that with the help of drainage channels, these entrances are limited throughout this layer. In order to strengthen the interpretation, a D10 DCR profile close to the coastline is planned. The resistivity values of the inverted data can be seen as close to and below 1 Ω m in Figs. 8 and 10. Salinity in the uppermost layer is similarly observed in the D11, D12 and D20 DCR resistivity profiles.

Water samples collected by Arslan and Demir (2013) were used for hydrochemical evaluation of the studied aquifer. For the characterization of the salinization and its sources, major ions, proportions of major ions, SAR, TDS and EC values were used and mapped (Fig. 5). Especially considering the results of the sodium, chlorine, SAR and TDS analysis (when the limits of saline and highly brackish zones are followed), hydrochemical data seems to be in close relationship to the low resistivity values observed near the surface in the final resistivity models (Fig. 12). In Fig. 6, we also mapped the total salinization criteria to see the possibility of saltwater intrusion. It is seen that some criteria are not met in the inner parts, whereas all the criteria are met in the sections close to the coastline where the surface resistivity is low. It is safe to assume that saltwater intrusion is occurring at the first aquifer levels in coastal regions, but this hazard is reduced through the inner parts of the study area due to both hydraulic gradient, pre-constructed drainage channels and recharge of the local phreatic aquifer from the local river. At the western part of the area, there is no information obtained from water quality analysis. Here, local farmers have been taking brackish or slightly fresh water from the sandy and gravelly units of the alluvium in the first 10 m. This can be confirmed from the DCR cross sections related to the relatively high resistivity values.

5. Conclusions

Evidence based on geological, geochemical and geophysical observations that groundwater of Bafra Plain has already been contaminated by seawater encroachment is presented in this paper. Geochemical data provided a direct (quantitative) characterization of the aquifer and proved to be the most accurate for groundwater quality determination, but sampling was conducted only where boreholes existed, and the spatial distribution was not optimal. Multi-geophysical measurements (DCR, TEM and RS) were collected and interpreted to provide an indirect characterization (qualitative characteristics) of the aquifer and salinization of the study area.

This work emphasizes that multidisciplinary approaches are needed in groundwater resource assessment. The reliability of the data (geophysical and geochemical) collected, the portable nature of the equipment, the fast data gathering and the minimal participants needed make this multi-proxy approach (quantitative and qualitative) an excellent tool for hydrogeology. After the integrated interpretation of all available data, it was concluded that seawater was the source of contamination at the northeastern part of Bafra Plain, and the seawater front was mapped. There is a significant salinization problem in the study area. We determined that saltwater intrusion is occurring inland up to 3.5 km, using multiple geophysical data sets guided by hydrogeological and hydrogeochemical data. After approximately the first 10 m depth, saltwater intrusion occurs in the plain. Freshwater can also be taken from the aquifers up to the first 10 m from the surface, which is close to the river. However, managers and policymakers must monitor it carefully. Otherwise, it is believed that the saltwater intrusion can move more toward the inner parts if groundwater extraction is not controlled, especially in the parts close to the river.

Nevertheless, climate change and/or increasing water demand (increasing pumping rates) could easily lead to a shortage of freshwater supplies, and increased salinization of the aquifers of the study area. For that reason, a multi-method approach is needed to find solutions for water management in order to achieve and preserve long-term protection of the available groundwater resources of the area.

Publisher's Note Springer Nature remains neutral with regard to jurisdictional claims in published maps and institutional affiliations.

References

Akpan, A. E., Ugbaja, A. N., & George, N. J. (2013). Integrated geophysical, geochemical and hydrogeological investigation of shallow groundwater resources in parts of the Ikom-Mamfe Embayment and the adjoining areas in Cross River State, Nigeria. *Environmental Earth Sciences, 70*(3), 1435–1456. https://doi.org/10.1007/s12665-013-2232-3.

Al-Garni, M. A., & El-Kaliouby, H. M. (2011). Delineation of saline groundwater and seawater intrusion zones using transient electromagnetic (TEM) method, Wadi Thuwal area, Saudi Arabia. *Arabian Journal of Geosciences, 4*(3–4), 655–668. https://doi.org/10.1007/s12517-009-0094-5.

Andreasen, D. C., & Fleck, W. B. (1997). Use of bromide: Chloride ratios to differentiate potential sources of chloride in a shallow, unconfined aquifer affected by brackish-water intrusion. *Hydrogeology Journal, 5*(2), 17–26. https://doi.org/10.1007/s100400050104.

Archie, G.E. (1942). The electrical resistivity log as an aid in determining some reservoir characteristics, American Institute of Mineral and Metal Engineering. Technical Publication 1422, *Petroleum Technology*, pp. 8–13.

Ardali, A. S., Tezkan, B., & Gürer, A. (2018). On the salt water intrusion into the Durusu Lake, Istanbul: A joint central loop TEM and multi-electrode ERT field survey. *Pure and Applied Geophysics, 175*(8), 3037–3050.

Arslan, H. (2012). Spatial and temporal mapping of groundwater salinity using ordinary kriging and indicator kriging: The case of Bafra Plain, Turkey. *Agricultural Water Management, 113,* 57–63. https://doi.org/10.1016/j.agwat.2012.06.015.

Arslan, H. (2013). Application of multivariate statistical techniques in the assessment of groundwater quality in seawater intrusion area in Bafra Plain, Turkey. *Environmental Monitoring and Assessment, 185*(3), 2439–2452. https://doi.org/10.1007/s10661-012-2722-x.

Arslan, H., Cemek, B., & Demir, Y. (2012). Determination of seawater intrusion via hydrochemicals and isotopes in Bafra Plain, Turkey. *Water Resources Management, 26*(13), 3907–3922. https://doi.org/10.1007/s11269-012-0112-3.

Arslan, H., & Demir, Y. (2011). Monitoring and assessing groundwater level by GIS: A case study in the irrigated soils of Bafra plain in Northern Turkey. *Anadolu Tarım Bilimleri Dergisi, 26*(3), 203–211.

Arslan, H., & Demir, Y. (2013). Impacts of seawater intrusion on soil salinity and alkalinity in Bafra Plain, Turkey. *Environmental Monitoring and Assessment, 185*(2), 1027–1040. https://doi.org/10.1007/s10661-012-2611-3.

Arslan, H., Güler, M., Cemek, D., & Demir, Y. (2007). Bafra ovası yeraltı suyu kalitesinin sulama açısından değerlendirilmesi. *JOTAF/Tekirdağ Ziraat Fakültesi Dergisi, 4*(2), 219–226.

Auken, E., Kirkegaard, C., Ribeiro, J., Foged, N., & Kok, A. (2010). The use of airborne electromagnetic for efficient mapping of salt water intrusion and outflow to the sea. In *SWIM21—21st Salt Water Intrusion Meeting* (pp. 21–26). http://www.swim-site.nl/pdf/swim21/pages_053_056.pdf. Accessed 25 Oct 2018.

Ayers, R.S., & Westcott, D.W. (1985). *Water Quality for Agriculture*. FAO Irrigation and Drainage Paper 29. Food and Agriculture Organization of the United Nations, Rome.

Barlow, P. M., & Reichard, E. G. (2010). Saltwater intrusion in coastal regions of North America. *Hydrogeology Journal, 18*(1), 247–260. https://doi.org/10.1007/s10040-009-0514-3.

Bashitialshaaer, R., Persson, K.M., & Larson, M.A. (2009). Estimated future production of desalinated seawater in the MENA countries and consequences for the recipients. In *World Congress & Water Reuse, Nov. 7–12, Dubai, United Arab Emirates*. http://portal.research.lu.se/ws/files/6091234/1507924.pdf. Accessed 25 Oct 2018.

Burnett, B., Chanton, J., Christoff, J., Kontar, E., Krupa, S., Lambert, M., et al. (2002). Assessing methodologies for measuring groundwater discharge to the ocean. *Eos, Transactions American Geophysical Union, 83*(11), 117–123. https://doi.org/10.1029/2002EO000069.

Capizzi, P., Cellura, D., Cosentino, P., Fiandaca, G., Martorana, R., Messina, P., et al. (2010). Integrated hydrogeochemical and geophysical surveys for a study of sea-water intrusion. *Bollettino di Geofisica Teoricaed Applicata, 51*(4), 285–300.

Cemek, B., Güler, M., Kiliç, K., Demir, Y., & Arslan, H. (2007). Assessment of spatial variability in some soil properties as related to soil salinity and alkalinity in Bafra plain in northern Turkey. *Environmental Monitoring and Assessment, 124*(1–3), 223–234. https://doi.org/10.1007/s10661-006-9220-y.

Choudhury, K., & Saha, D. K. (2004). Integrated geophysical and chemical study of saline water intrusion. *Groundwater, 42*(5), 671–677. https://doi.org/10.1111/j.1745-6584.2004.tb02721.x.

Choudhury, K., Saha, D. K., & Chakraborty, P. (2001). Geophysical study for saline water intrusion in a coastal alluvial terrain. *Journal of Applied Geophysics, 46*(3), 189–200. https://doi.org/10.1016/S0926-9851(01)00038-6.

Clifton, C., Evans, R., Hayes, S., Hirji, R., Puz, G., & Pizarro, C. (2010). *Water and Climate Change: Impacts on Groundwater Resources and Adaptation Options*. Water Working Notes; No. 25. World Bank, Washington, DC. © World Bank. License: CC BY 3.0 IGO. https://openknowledge.worldbank.org/handle/10986/27857. Accessed 10 Jan 2020.

Demirci, İ., Candansayar, M. E., Vafidis, A., & Soupios, P. (2017). Two dimensional joint inversion of direct current resistivity, radio-magnetotelluric and seismic refraction data: An application from Bafra Plain, Turkey. *Journal of Applied Geophysics, 139,* 316–330. https://doi.org/10.1016/j.jappgeo.2017.03.002.

Demirci, I., Erdoğan, E., & Candansayar, M. E. (2012). Two-dimensional inversion of direct current resistivity data incorporating topography by using finite difference techniques with triangle cells: Investigation of Kera fault zone in western Crete. *Geophysics, 77*(1), E67–E75. https://doi.org/10.1190/geo2011-0130.1.

EPA. (1986). *Quality criteria for water 1986.* EPA 440/5-86-001. Washington, DC: US Environmental Protection Agency.

Ezersky, M., Legchenko, A., Al-Zoubi, A., Levi, E., Akkawi, E., & Chalikakis, K. (2011). TEM study of the geoelectrical structure and groundwater salinity of the Nahal Hever sinkhole site, Dead Sea shore, Israel. *Journal of Applied Geophysics, 75*(1), 99–112. https://doi.org/10.1016/j.jappgeo.2011.06.011.

Farid, A., Khalid, P., Jadoon, K. Z., & Jouini, M. S. (2014). The depositional setting of the Late Quaternary sedimentary fill in southern Bannu basin, Northwest Himalayan fold and thrust belt, Pakistan. *Environmental Monitoring and Assessment, 186*(10), 6587–6604. https://doi.org/10.1007/s10661-014-3876-5.

FitzGerald, D. M., Fenster, M. S., Argow, B. A., & Buynevich, I. V. (2008). Coastal impacts due to sea-level rise. *Annual Review of Earth and Planetary Sciences, 36,* 601–647. https://doi.org/10.1146/annurev.earth.35.031306.140139.

Foged, N., Auken, E., Christiansen, A. V., & Sørensen, K. I. (2013). Test-site calibration and validation of airborne and ground-based TEM systems. *Geophysics, 78*(2), E95–E106. https://doi.org/10.1190/geo2012-0244.1.

Goebel, M., Pidlisecky, A., & Knight, R. (2017). Resistivity imaging reveals complex pattern of saltwater intrusion along Monterey coast. *Journal of Hydrology, 551,* 746–755. https://doi.org/10.1016/j.jhydrol.2017.02.037.

Golshan, M., Colombani, N., & Mastrocicco, M. (2018). Assessing aquifer salinization with multiple techniques along the Southern Caspian Sea Shore (Iran). *Water, 10*(4), 348. https://doi.org/10.3390/w10040348.

Green, T. R. (2016). Linking climate change and groundwater. In A. J. Jakeman, O. Barreteau, R. J. Hunt, J. D. Rinaudo, & A. Ross (Eds.), *Integrated groundwater management*. Cham: Springer.

Güler, M., Arslan, H., Cemek, B., & Erşahin, S. (2014). Long-term changes in spatial variation of soil electrical conductivity and exchangeable sodium percentage in irrigated mesic ustifluvents. *Agricultural Water Management, 135,* 1–8. https://doi.org/10.1016/j.agwat.2013.12.011.

Hamdan, H. A., & Vafidis, A. (2013). Joint inversion of 2D resistivity and seismic travel time data to image saltwater intrusion over karstic areas. *Environmental Earth Sciences, 68*(7), 1877–1885. https://doi.org/10.1007/s12665-012-1875-9.

Himi, M., Tapias, J., Benabdelouahab, S., Salhi, A., Rivero, L., Elgettafi, M., et al. (2017). Geophysical characterization of saltwater intrusion in a coastal aquifer: The case of Martil-Alila plain (North Morocco). *Journal of African Earth Sciences, 126,* 136–147. https://doi.org/10.1016/j.jafrearsci.2016.11.011.

Kalisperi, D., Kouli, M., Vallianatos, F., Soupios, P., Kershaw, S., & Lydakis-Simantiris, N. (2018). A transient electromagnetic (TEM) method survey in north-central coast of Crete, Greece:

Evidence of seawater intrusion. *Geosciences, 8*(4), 107. https://doi.org/10.3390/geosciences8040107.

Kanta, A., Soupios, P., Barsukov, P., Kouli, M., & Vallianatos, F. (2013). Aquifer characterization using shallow geophysics in the Keritis Basin of Western Crete, Greece. *Environmental Earth Sciences, 70*(5), 2153–2165. https://doi.org/10.1007/s12665-013-2503-z.

Karaalioğlu, B., & İslamoğlu, M. (1988). *Bafra Ovası Hidrojeolojik Etüd Raporu*. General Directorates of Hydraulic Work, Samsun, Turkey (pp. 1–44).

Khalil, M. A., Abbas, A. M., Santos, F. M., Masoud, U., & Salah, H. (2013). Application of VES and TDEM techniques to investigate sea water intrusion in Sidi Abdel Rahman area, northwestern coast of Egypt. *Arabian Journal of Geosciences, 6*(8), 3093–3101. https://doi.org/10.1007/s12517-012-0564-z.

Kourgialas, N. N., Dokou, Z., Karatzas, G. P., Panagopoulos, G., Soupios, P., Vafidis, A., et al. (2016). Saltwater intrusion in an irrigated agricultural area: Combining density-dependent modeling and geophysical methods. *Environmental Earth Sciences, 75*(1), 15. https://doi.org/10.1007/s12665-015-4856-y.

Kumar, V. S., Dhakate, R., Amarender, B., & Sankaran, S. (2016). Application of ERT and GPR for demarcating the saline water intrusion in coastal aquifers of Southern India. *Environmental Earth Sciences, 75*(5), 1–17. https://doi.org/10.1007/s12665-015-5207-8.

Kura, N. U., Ramli, M. F., Ibrahim, S., Sulaiman, W. N. A., & Aris, A. Z. (2014). An integrated assessment of seawater intrusion in a small tropical island using geophysical, geochemical, and geostatistical techniques. *Environmental Science and Pollution Research, 21*(11), 7047–7064. https://doi.org/10.1007/s11356-014-2598-0.

Larsen, F., Tran, L. V., Van Hoang, H., Tran, L. T., Christiansen, A. V., & Pham, N. Q. (2017). Groundwater salinity influenced by Holocene seawater trapped in incised valleys in the Red River delta plain. *Nature Geoscience, 10*(5), 376. https://doi.org/10.1038/ngeo2938.

Leedshill, B., Bechtel, I., Ias, G., & Gizbili, M. (1965). *Feasibility report of Bafra project*. Ankara: General Directorates of Hydraulic Work.

Martens, S., & Wichmann, K. (2007). Groundwater salinisation. In J. L. Lozán, H. Grassl, P. Hupfer, L. Menzel. C. D. Schönwiese (Eds.), *Global change: Enough water for all?* Wissenschaftliche Auswertungen, Hamburg. 384 S. Online: http://www.klimawarnsignale.uni-hamburg.de. Accessed 25 Oct 2018.

Massoud, U., Kenawy, A. A., Ragab, E. S. A., Abbas, A. M., & El-Kosery, H. M. (2014). Characterization of the groundwater aquifers at El Sadat City by joint inversion of VES and TEM data. *NRIAG Journal of Astronomy and Geophysics, 3*(2), 137–149. https://doi.org/10.1016/j.nrjag.2014.10.001.

Milly, P. C., Dunne, K. A., & Vecchia, A. V. (2005). Global pattern of trends in streamflow and water availability in a changing climate. *Nature, 438*(7066), 347–350. https://doi.org/10.1038/nature04312.

MTA. (2006). *Geological map of Turkey, 1/100.000 scaled Sinop E35 quadrangle, compiled by Mustafa Sevin and M. Fuat Uğuz*. Ankara: General Directorate of Mineral Research and Exploration (MTA).

Murgulet, D., & Tick, G. (2008). The extent of saltwater intrusion in southern Baldwin County, Alabama. *Environmental Geology, 55*(6), 1235–1245. https://doi.org/10.1007/s00254-007-1068-0.

Nordstrom, D. K., Lindblom, S., Donahoe, R. J., & Barton, C. C. (1989). Fluid inclusions in the Stripa granite and their possible influence on the groundwater chemistry. *Geochimica et Cosmochimica Acta, 53*(8), 1741–1755.

Olivares, E. A. O., Torres, S. S., Jimenez, S. I. B., Enriquez, J. O. C., Zignol, F., Reygadas, Y., et al. (2019). Climate change, land use/land cover change, and population growth as drivers of groundwater depletion in the central valleys, Oaxaca, Mexico. *Remote Sensing, 11,* 1290. https://doi.org/10.3390/rs11111290.

Olutoge, F. A., & Amusan, G. M. (2014). The effect of sea water on compressive strength of concrete. *International Journal of Engineering Science Invention, 3*(7), 23–31.

Patra, H. P., & Bhattacharya, P. K. (1966). Geophysical exploration for ground water around Digha in the coastal region of West Bengal, India. *Geoexploration, 4*(4), 209–218. https://doi.org/10.1016/0016-7142(66)90019-6.

Petalas, C.P. (1997). *Analysis of aquifer systems in the heterogeneous coastal plain of Rhodope region*. PhD, University of Thrace, Department of Civil Engineering, Xanthi, Greece.

Post, V. E. A. (2005). Fresh and saline groundwater interaction in coastal aquifers: Is our technology ready for the problems ahead? *Hydrogeology Journal, 13*(1), 120–123. https://doi.org/10.1007/s10040-004-0417-2.

Rani, P., Piegari, E., Di Maio, R., Vitagliano, E., Soupios, P., & Milano, L. (2019). Monitoring time evolution of self-potential anomaly sources by a new global optimization approach. Application to organic contaminant transport. *Journal of Hydrology, 575,* 955–964.

Redhaounia, B., Aktarakçi, H., Ilondo, B. O., Gabtni, H., Khomsi, S., & Bédir, M. (2015). Hydro-geophysical interpretation of fractured and karstified limestones reservoirs: A case study from Amdoun region (NW Tunisia) using electrical resistivity tomography, digital elevation model (DEM) and hydro-geochemical approaches. *Journal of African Earth Sciences, 112,* 328–338. https://doi.org/10.1016/j.jafrearsci.2015.09.020.

Sabet, M. A. (1975). Vertical electrical resistivity sounding locate groundwater resources: A feasibility study. Virginia Polytechnical Institute. *Water Resources Bulletin, 73,* 63.

Samsudin, A. R., Haryono, A., Hamzah, U., & Rafek, A. G. (2008). Salinity mapping of coastal groundwater aquifers using hydrogeochemical and geophysical methods: A case study from north Kelantan, Malaysia. *Environmental Geology, 55*(8), 1737–1743. https://doi.org/10.1007/s00254-007-1124-9.

Small, C., & Nicholls, R. J. (2003). A global analysis of human settlement in coastal zones. *Journal of Coastal Research, 19*(3), 584–599.

Somay, M. A., & Gemici, Ü. (2009). Assessment of the salinization process at the coastal area with hydrogeochemical tools and geographical information systems (GIS): Selçuk plain, Izmir, Turkey. *Water, Air, and Soil Pollution, 201*(1–4), 55–74. https://doi.org/10.1007/s11270-008-9927-1.

Soupios, P. M., Kalisperi, D., Kanta, A., Kouli, M., Barsukov, P., & Vallianatos, F. (2010). Coastal aquifer assessment based on geological and geophysical survey, northwestern Crete, Greece. *Environmental Earth Sciences, 61*(1), 63–77. https://doi.org/10.1007/s12665-009-0320-1.

Soupios, P., Nektarios, K., Zoi, D., George, K., George, P., Antonis, V., et al. (2015). Modeling saltwater intrusion at an agricultural coastal area using geophysical methods and the FEFLOW model. *Engineering Geology for Society and Territory, 3,* 249–252. https://doi.org/10.1007/978-3-319-09054-2_51.

Trabelsi, F., Mammou, A. B., Tarhouni, J., Piga, C., & Ranieri, G. (2013). Delineation of saltwater intrusion zones using the time domain electromagnetic method: The Nabeul–Hammamet coastal aquifer case study (NE Tunisia). *Hydrological Processes, 27*(14), 2004–2020. https://doi.org/10.1002/hyp.9354.

USDA-United States Department of Agriculture. (1954). *Diagnosis and Improvement of Saline and Alkali Soils Handbook No. 60.* Editor: Richards, L. A. https://www.ars.usda.gov/ARSUserFiles/20360500/hb60_pdf/hb60complete.pdf. Accessed 25 Oct 2018.

Vafidis, A., Soupios, P., Economou, N., Hamdan, H., Andronikidis, N., Kritikakis, G., et al. (2014). Seawater intrusion imaging at Tybaki, Crete, using geophysical data and joint inversion of electrical and seismic data. *First Break, 32*(8), 107–114.

Vörösmarty, C. J., Green, P., Salisbury, J., & Lammers, R. B. (2000). Global water resources: Vulnerability from climate change and population growth. *Science, 289*(5477), 284–288. https://doi.org/10.1126/science.289.5477.284.

Wiederhold, H., Sulzbacher, H., Grinat, M., Günther, T., Igel, J., Burschill, T., & Siemon, B. (2013). Hydrogeophysical characterization of freshwater/saltwater systems—case study: Borkum Island, Germany. *First Break, August*(8), 109–117.

Yan, S., Xue, G. Q., Qiu, W. Z., Li, H., & Zhong, H. S. (2016). Feasibility of central loop TEM method for prospecting multi-layer water-filled goaf. *Applied Geophysics, 13*(4), 587–597. https://doi.org/10.1007/s11770-016-0586-5.